A Gain-Adaptive High-Order Terminal Sliding Mode Observer Under SPMSM Sensorless Control

Chonghui Song, *Member, IEEE*, Wenbing Hu, Jiayan Zhang, Chunwang Zhao, and Xianrui Sun

***Abstract*—In this article, a gain-adaptive (GA) high-order terminal sliding mode observer (HOTSMO) is designed for back-electromotive force (back-EMF) estimation in the sensorless control of permanent magnet synchronous motors. The proposed observer features an adaptive gain mechanism that dynamically adjusts the sliding mode gain coefficient based on the system state. During the reaching phase with large observation errors, the gain coefficient is elevated to ensure observer stability. As the system approaches the sliding surface, the gain coefficient automatically reduces to suppress chattering while maintaining estimation accuracy. The adaptive mechanism is achieved through real-time coordination between the sliding mode surface function and the gain coefficient. Compared with the conventional HOTSMO, the proposed GA-HOTSMO effectively suppresses chattering and reduces both current and back-EMF estimation errors while maintaining observer stability. The effectiveness of the proposed GA-HOTSMO is validated through comprehensive theoretical analysis and experimental results.**

***Index Terms*—Chattering suppression, finite-time convergence, gain adaptive (GA), high-order terminal sliding mode observer (HOTSMO), permanent magnet synchronous motor (PMSM), sensorless control.**

I. Introduction

SURFACE-MOUNTED permanent magnet synchronous motors (SPMSMs) have been widely used in industrial applications owing to the advantages of high efficiency, high power density, and high control accuracy [1]. However, the high cost, large size, and poor stability of high-precision mechanical position sensors result in increased expense, extra space occupation, and decreased reliability, sensorless control of permanent magnet synchronous motors (PMSMs) has been receiving increasing attention [2]. The model-based PMSM sensorless control framework has been widely applied in medium and high-speed regions [3], [4], [5], [6]. In the sensorless control framework, the performance of observers plays a key role in the control system, such as sliding mode observers (SMOs) [7], [8], [9], [10], model reference adaptive observers [11], full-order observers [12], and extended Kalman filter observers [13]. Among these methods, SMO has advantages of strong robustness and fast convergence. However, the chattering problem caused by discontinuous control law is an inherent drawback of SMO [14]. Moreover, the traditional linear sliding mode surface cannot achieve finite-time convergence of state variables [15]. Thus, chattering and nonfinite-time convergence are two key issues limiting the application of SMO. Gain-adaptive (GA) control has been studied in [16], [17], [18], and [19], but most of them are applied to sliding mode controllers or low-order SMOs, and few have been applied to high-order terminal sliding mode observers (HOTSMO). The idea of gain adaptation can further reduce the chattering effect of SMOs.

First, concerning the chattering suppression problem of SMO, Comanescu [20] smoothed the discontinuous control law by adding a low-pass filter (LPF), but the introduction of LPF inevitably leads to phase delay and amplitude error. Wang et al. [21] proposed an extended SMO to suppress chattering. However, it can only guarantee the convergence of stator current error term, not the convergence of the stator current error derivative term. This results in errors in the estimated back-electromotive force (back-EMF) and extracted rotor position.

Second, in light of the problem that SMO is unable to achieve finite-time convergence, Wang et al. [22] improved the convergence rate by using exponential control law, but could not achieve finite-time convergence, resulting in steady-state errors in the system. Lee et al. [23] introduced an integral sliding mode surface applicable to continuous control law to achieve finite-time convergence, but sacrificed the robustness of SMO. Wang et al. [24] proposed a high-order sliding mode load torque observer to achieve finite-time convergence. However, since the load torque observer is only used for feedforward compensation in the speed loop, it cannot be directly applied to SPMSM position estimation. In [25], a hybrid terminal SMO was proposed, but it is only applicable to first-order SPMSM models. Moreover, its rotor position is calculated in open-loop based on the estimated back-EMF, which is very sensitive to system noise. In [26], an HOTSMO was proposed, addressing the disadvantage that traditional extended SMO back-EMF error cannot achieve finite-time convergence to zero. Although the designed terminal sliding mode surface and high-order control law achieved finite-time convergence of stator current error and

Received 17 July 2024; revised 24 October 2024; accepted 28 December 2024. Date of publication 3 January 2025; date of current version 26 February 2025. This work was supported by the Youth Research Projects of Liaoning Provincial Education Department under Grant LJ212410149034. Recommended for publication by Associate Editor R. Kennel. *(Corresponding author: Chonghui Song.)*

Chonghui Song, Wenbing Hu, Jiayan Zhang, and Chunwang Zhao are with the College of Information Science and Engineering, Northeastern University, Shenyang 110819, China (e-mail: chonghui.song@gmail.com; 2310256@stu.edu.cn; zjy1115787@163.com; zhao194196@163.com).

Xianrui Sun is with the College of Information Engineering, Shenyang University of Chemical Technology, Shenyang 110142, China (e-mail: xian.ruisun@163.com).

Color versions of one or more figures in this article are available at https://doi.org/10.1109/TPEL.2025.3525550.

Digital Object Identifier 10.1109/TPEL.2025.3525550

observed back-EMF, the control law gain needs to be balanced in terms of chattering suppression, ensuring observer stability, and system dynamic performance. Therefore, although a larger gain coefficient ensures observer stability, it causes system overshoot and severe oscillations, thus reducing closed-loop system stability. Hence, effectively reducing chattering while ensuring observer stability is an urgent problem to be solved.

Therefore, this article proposes a gain-adaptive high-order terminal sliding mode observer (GA-HOTSMO) that suppresses chattering while improving the estimation accuracy of back-EMF and rotor position, and also ensures finite-time convergence. To address the problem that the control law gain coefficient designed in [26] needs to be set to a larger value to satisfy the stability of the observer, which leads to larger chattering, this article introduces a sliding mode surface function term in the gain coefficient. The gain coefficient will adaptively adjust with the change of the sliding mode surface function, further weakening chattering. When the observation error is large, the gain coefficient will automatically adjust to a larger value with the sliding mode surface function to ensure observer stability; when the observation error decreases, the gain coefficient will automatically adjust to a smaller value to weaken system chattering. Therefore, the real-time GA-HOTSMO proposed in this article can achieve finite-time convergence, effectively reduce chattering, decrease overshoot, and improve system dynamic performance.

II. HOTSMO Problem Analysis

Fig. 1 represents the two-level power topology and its SVC framework of SPMSM. In the $\alpha\beta$ stationary coordinate system, the SPMSM mathematical model is as follows [21]:

$$\frac{d}{dt}\begin{bmatrix} i_\alpha \\ i_\beta \end{bmatrix} = \begin{bmatrix} -\frac{R_s}{L_s} & 0 \\ 0 & -\frac{R_s}{L_s} \end{bmatrix}\begin{bmatrix} i_\alpha \\ i_\beta \end{bmatrix} + \frac{1}{L_s}\begin{bmatrix} u_\alpha - e_\alpha \\ u_\beta - e_\beta \end{bmatrix} \quad (1)$$

where i_α and i_β are the stator currents on the $\alpha\beta$ axes, u_α and u_β are the stator voltage components on the $\alpha\beta$ axes, L_s is the stator inductance, R_s is the stator resistance, and e_α and e_β are the back-EMF components on the $\alpha\beta$ axes

$$\begin{bmatrix} e_\alpha \\ e_\beta \end{bmatrix} = \omega_e \psi_f \begin{bmatrix} -\sin\theta_e \\ \cos\theta_e \end{bmatrix} \quad (2)$$

where ω_e is the electrical angular speed, ψ_f is the permanent magnet flux linkage, and θ_e is the rotor electrical angle.

From (1)

$$\frac{d\mathbf{i}}{dt} = \mathbf{A}\mathbf{i} + \mathbf{B}(\mathbf{u} - \mathbf{e}) \quad (3)$$

where $\mathbf{i} = [i_\alpha\ i_\beta]^T$, $\mathbf{u} = [u_\alpha\ u_\beta]^T$, $\mathbf{e} = [e_\alpha\ e_\beta]^T$, $\mathbf{A} = -\frac{R_s}{L_s}\mathbf{I}$, $\mathbf{B} = \frac{1}{L_s}\mathbf{I}$, and $\mathbf{I} = \begin{bmatrix} 1 & 0 \\ 0 & 1 \end{bmatrix}$.

In the SVC, in order to obtain the estimated speed, an SMO can be used to observe e. Nevertheless, without compromising system robustness, the conventional SMO based on the first-order model struggles to provide chattering suppression and precise rotor position estimate.

In PMSM systems, the mechanical time constant is significantly larger than the electrical time constant, resulting in slower

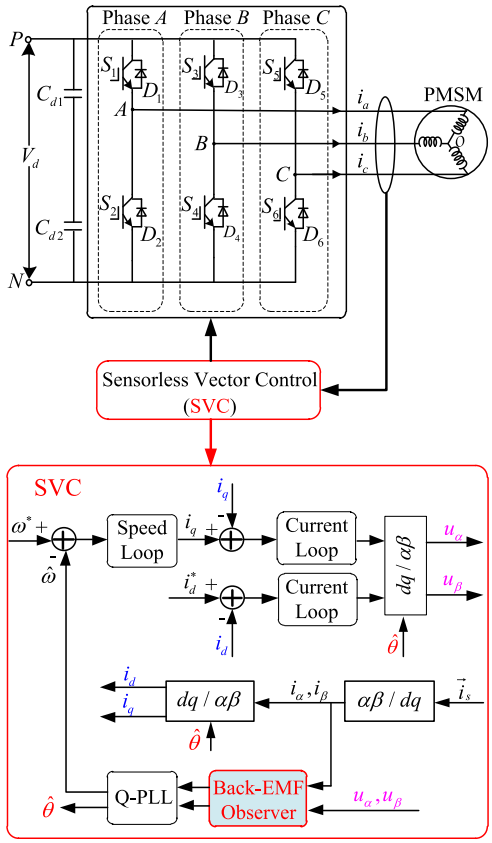

Fig. 1. Two-level drive system topology of PMSM.

rotor speed variations compared to electrical dynamics [21], [30]. Therefore, assume that $d\omega_e/dt = 0$, meaning the rotor speed can be considered constant during the electrical transient analysis. By treating $\mathbf{e}$ in (3) as an extended state, the extended mathematical model of SPMSM is established [21]

$$\frac{d}{dt}\begin{bmatrix} \mathbf{i} \\ \mathbf{e} \end{bmatrix} = \begin{bmatrix} \mathbf{A}_{11} & \mathbf{A}_{12} \\ 0 & \mathbf{A}_{22} \end{bmatrix}\begin{bmatrix} \mathbf{i} \\ \mathbf{e} \end{bmatrix} + \begin{bmatrix} \mathbf{B} \\ 0 \end{bmatrix}\mathbf{u} \quad (4)$$

where $A_{11} = A$, $A_{12} = -B$, $\mathbf{A}_{22} = \omega_e\mathbf{J}$, $\mathbf{J} = \begin{bmatrix} 0 & -1 \\ 1 & 0 \end{bmatrix}$.

Although the extended SMO based on (4) achieves the convergence of current error, it cannot guarantee the convergence of the derivative term of observed current error, which leads to the inability to achieve finite-time convergence of back-EMF estimation and results in rotor position estimation errors. In order to achieve chattering suppression and finite-time convergence, the HOTSMO was proposed in [26]. The terminal sliding mode surface and the high-order sliding mode control law of the HOTSMO are represented by (5) and (6), respectively

$$\boldsymbol{s} = \frac{d\delta_{\boldsymbol{i}}}{dt} + \beta|\delta_{\boldsymbol{i}}|\text{sign}(\delta_{\boldsymbol{i}}) \quad (5)$$

$$Z_{\mathbf{i}} = -\beta \mid \delta_{\mathbf{i}} \mid^{\gamma} \text{sign}(\delta_{\mathbf{i}}) - \mathbf{u}_n$$

$$\frac{d\boldsymbol{u}_n}{dt} = -g\boldsymbol{u}_n + k\text{sign}(\mathbf{s}) \quad (6)$$

where $\boldsymbol{s}$ denotes the sliding mode surface of the HOTSMO, $Z_{\boldsymbol{i}} = [Z_{i_\alpha}\ Z_{i_\beta}]^T$ represents the control law of the HOTSMO, $\delta_{\boldsymbol{i}} =$

$[\delta_{i_\alpha}\ \delta_{i_\beta}]^T$ indicates the stator current error, sign() represents the sign function, and g, k, β, γ are controller gains.

Combining the sliding mode surface and control law, the HOTSMO mathematical model is as follows:

$$\frac{d}{dt}\begin{bmatrix}\hat{\mathbf{i}}\\ \hat{\mathbf{e}}\end{bmatrix} = \begin{bmatrix}\mathbf{A_{11}} & \mathbf{A}_{12}\\ 0 & \hat{\mathbf{A}}_{22}\end{bmatrix}\begin{bmatrix}\hat{\mathbf{i}}\\ \hat{\mathbf{e}}\end{bmatrix} + \begin{bmatrix}\mathbf{B}\\ 0\end{bmatrix}\mathbf{u} + \begin{bmatrix}Z_{\boldsymbol{i}}\\ \Delta\end{bmatrix} \tag{7}$$

where $\hat{}$ represents the estimated value, $\hat{\mathbf{A}}_{22} = \hat{\omega}_e\mathbf{J}$, $\hat{\omega}_e$ is the observed electrical angular velocity, and

$$\Delta = [m\,\mathrm{sign}(s_\alpha)\ m\,\mathrm{sign}(s_\beta)]^T \tag{8}$$

where m is the gain coefficient.

In [26], to achieve stable conditions, k and m in HOTSMO should satisfy

$$\begin{cases} k > \max\left(|A_{11}D| + |gu_{n\alpha}|, |A_{11}D| + |gu_{n\beta}|\right) \\ m > \max\left(|\hat{\omega}_e\delta_{e_\alpha}|, |\hat{\omega}_e\delta_{e_\beta}|\right) \end{cases} \tag{9}$$

where $\delta_{\mathbf{e}} = [\delta_{e_\alpha}\ \delta_{e_\beta}]^T$ is the back-EMF error and D is the upper bound of the current differential error satisfying [25]

$$0 \le \max\left(\left|\frac{d\delta_{i_\alpha}}{dt}\right|, \left|\frac{d\delta_{i_\beta}}{dt}\right|\right) \le D. \tag{10}$$

Since the sliding mode surface function $\mathbf{s}$ contains not only the current error term but also the derivative term of the current error, after the observer are stabilized, it ensures the convergence of the observed current error term and the current error derivative term.

However, when selecting the gain coefficients for HOTSMO, if a larger gain coefficient is chosen to ensure the stability of the observer, then chattering increases and the system's dynamic performance deteriorates. On the other hand, if a smaller gain coefficient is chosen to suppress chattering, although it improves the system's dynamic performance, it cannot guarantee the stability of the observer. When k and m satisfy (9), HOTSMO is stable, but k and m are fixed values and need to be greater than the product of the maximum back-EMF error and estimated electrical angular velocity throughout the control period. When the observation error is in the process of approaching the sliding mode surface, the observed back-EMF error is relatively large, and a larger m value is required to satisfy the stability condition of the observer. However, a larger gain coefficient will cause greater chattering, leading to a larger observed back-EMF error, and thus resulting in a larger error in the extracted speed and position information from the phase-locked loop. That is, the stability of the observer is achieved at the expense of sacrificing system dynamic performance and increasing chattering.

Therefore, this article proposes a real-time GA-HOTSMO, which can achieve the stability and finite-time convergence of the observer while improving system dynamic performance and reducing chattering.

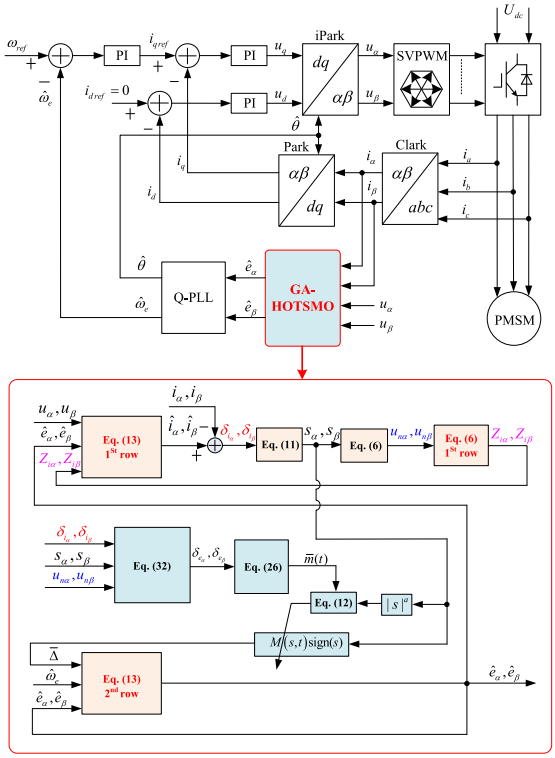

Fig. 2. Framework of the SPMSM sensorless control system.

III. GA-HOTSMO Design

A. GA-HOTSMO Model Built

The terminal sliding mode surface of GA-HOTSMO is designed as

$$\mathbf{s} = \begin{bmatrix}s_\alpha\\ s_\beta\end{bmatrix} = \frac{d}{dt}\begin{bmatrix}\delta_{i_\alpha}\\ \delta_{i_\beta}\end{bmatrix} + \beta\begin{bmatrix}|\delta_{i_\alpha}|^\gamma \mathrm{sign}(\delta_{i_\alpha})\\ |\delta_{i_\beta}|^\gamma \mathrm{sign}(\delta_{i_\beta})\end{bmatrix} \tag{11}$$

where $\beta > 0$ and $0 < \gamma < 1$.

Define the adaptive function

$$M(s,t) = \bar{m}(t)\begin{bmatrix}\epsilon + |s_\alpha|^a & 0\\ 0 & \epsilon + |s_\beta|^a\end{bmatrix} \tag{12}$$

where ϵ is a very small positive number, a is the power exponent, $\bar{m}(t)$ is the adaptive adjusting coefficient, and $M(\mathbf{s},t)$ will adaptively adjust according to $\mathbf{s}$.

The SPMSM model for GA-HOTSMO is

$$\frac{d}{dt}\begin{bmatrix}\hat{\mathbf{i}}\\ \hat{\mathbf{e}}\end{bmatrix} = \begin{bmatrix}\mathbf{A_{11}} & \mathbf{A}_{12}\\ 0 & \hat{\mathbf{A}}_{22}\end{bmatrix}\begin{bmatrix}\hat{\mathbf{i}}\\ \hat{\mathbf{e}}\end{bmatrix} + \begin{bmatrix}\mathbf{B}\\ 0\end{bmatrix}\mathbf{u} + \begin{bmatrix}Z_{\mathbf{i}}\\ \bar{\Delta}\end{bmatrix} \tag{13}$$

where $Z_{\mathbf{i}}$ is the same as in (6) and

$$\bar{\Delta} = \begin{bmatrix}M(s_\alpha,t)\,\mathrm{sign}(s_\alpha)\\ M(s_\beta,t)\,\mathrm{sign}(s_\beta)\end{bmatrix}. \tag{14}$$

Fig. 2 depicts the block diagram of the SPMSM sensorless drive based on FOC using GA-HOTSMO and an improved quadrature-component-based phase-locked loop [27].

B. Stability Analysis of GA-HOTSMO

Choose the Lyapunov function as

$$V = \frac{1}{2}s^T s. \tag{15}$$

Differentiate (15)

$$\frac{dV}{dt} = s^T \frac{ds}{dt}. \tag{16}$$

According to the Lyapunov stability condition, $dV/dt < 0$ ensures the stability of the proposed observer.

Subtracting (4) from (13) yields the differential of stator current error, i.e.,

$$\frac{d\delta_{\mathbf{i}}}{dt} = \mathbf{A}_{11}\delta_{\mathbf{i}} + \mathbf{A}_{12}\delta_{\mathbf{e}} - \mathbf{u}_n - \beta\left|\delta_{\mathbf{i}}\right|^{\gamma}\operatorname{sign}\left(\delta_{\mathbf{i}}\right). \tag{17}$$

Substituting (17) into (11)

$$\mathbf{s} = \mathbf{A}_{11}\delta_{\mathbf{i}} + \mathbf{A}_{12}\delta_{\mathbf{e}} - \mathbf{u}_n. \tag{18}$$

In (13), considering that the mechanical time constant of a PMSM system is significantly larger than the electrical time constant, the electrical angular speed ω_e is assumed to be constant. However, during acceleration and deceleration, instantaneous speed estimation errors are inevitable [30]. Consequently, in the stability analysis, the assumption $\hat{\omega}_e = \omega_e$ may be overly restrictive. To verify the stability of the observer designed under this assumption, it is necessary to prove stability before the estimation error converges to zero. Thus, we define the speed estimation error as follows:

$$\delta_{\omega_e} = \hat{\omega}_e - \omega_e. \tag{19}$$

Subtracting (4) from (13) yields the differential of the back-EMF error

$$\begin{aligned}\frac{d\delta_{\mathbf{e}}}{dt} &= \hat{\mathbf{A}}_{22}\hat{\mathbf{e}} - \mathbf{A}_{22}\mathbf{e} + M(\mathbf{s},t)\operatorname{sign}(\mathbf{s}) \\ &= \delta_{\omega_e}\mathbf{J}\hat{\mathbf{e}} - \hat{\omega}_e\mathbf{J}\delta_e - \delta_{\omega_e}\mathbf{J}\delta_{\mathbf{e}} + M(\mathbf{s},t)\operatorname{sign}(\mathbf{s}).\end{aligned} \tag{20}$$

Substituting (6) and (20) into the derivative of (18)

$$\begin{aligned}\frac{d\mathbf{s}}{dt} =& -k\operatorname{sign}(\mathbf{s}) + \mathbf{A}_{11}\frac{d\delta_{\mathbf{i}}}{dt} + g\mathbf{u}_n \\ &+ \mathbf{A}_{12}(\delta_{\omega_e}\mathbf{J}\hat{\mathbf{e}} - \hat{\omega}_e\mathbf{J}\delta_e - \delta_{\omega_e}\mathbf{J}\delta_{\mathbf{e}} + M(\mathbf{s},t)\operatorname{sign}(\mathbf{s})).\end{aligned} \tag{21}$$

Substituting (21) into (16)

$$\frac{dV}{dt} = \mathbf{s}^T\begin{pmatrix} -k\operatorname{sign}(\mathbf{s}) + \mathbf{A}_{11}\frac{d\delta_{\mathbf{i}}}{dt} + \mathrm{g}\mathbf{u}_n + \mathbf{A}_{12}(\delta_{\omega_e}\mathbf{J}\hat{\mathbf{e}} \\ -\hat{\omega}_e\mathbf{J}\delta_e - \delta_{\omega_e}\mathbf{J}\delta_{\mathbf{e}} + M(\mathbf{s},t)\operatorname{sign}(\mathbf{s}))\end{pmatrix}. \tag{22}$$

After rearranging (22)

$$\begin{aligned}\frac{dV}{dt} =& -k|s_\alpha| + s_\alpha\left(-\frac{R_s}{L_s}\frac{d\delta_{i_\alpha}}{dt} + gu_{n\alpha}\right) \\ &-k|s_\beta| + s_\beta\left(-\frac{R_s}{L_s}\frac{d\delta_{i_\beta}}{dt} + gu_{n\beta}\right) \\ &-\frac{1}{L_s}(s_\alpha\hat{\omega}_e\delta_{e_\beta} + s_\alpha\bar{m}(t)(\epsilon + |s_\alpha|^a)\operatorname{sign}(s_\alpha)) \\ &-\frac{1}{L_s}(-s_\beta\hat{\omega}_e\delta_{e_\alpha} + s_\beta\bar{m}(t)(\epsilon + |s_\beta|^a)\operatorname{sign}(s_\beta)) \\ &-\frac{1}{L_s}(-s_\alpha\delta_{\omega_e}(\hat{e}_\beta - \delta_{e_\beta}) + s_\beta\delta_{\omega_e}(\hat{e}_\alpha - \delta_{e_\alpha})).\end{aligned} \tag{23}$$

Substituting (23) into (10), it can be obtained that

$$\begin{aligned}\frac{dV}{dt} <& -k|s_\alpha| + |s_\alpha|\left(\frac{R_s}{L_s}D + |gu_{n\alpha}|\right) \\ &-k|s_\beta| + |s_\beta|\left(\frac{R_s}{L_s}D + |gu_{n\beta}|\right) \\ &-\frac{1}{L_s}(s_\alpha\hat{\omega}_e\delta_{e_\beta} + s_\alpha\overline{m}(t)(\epsilon + |\ s_\alpha\ |^a)\operatorname{sign}(s_\alpha)) \\ &-\frac{1}{L_s}(-s_\beta\hat{\omega}_e\delta_{e_\alpha} + s_\beta\overline{m}(t)(\epsilon + |\ s_\beta\ |^a)\operatorname{sign}(s_\beta)) \\ &-\frac{1}{L_s}(-s_\alpha\delta_{\omega_e}(\hat{e}_\beta - \delta_{e_\beta}) + s_\beta\delta_{\omega_e}(\hat{e}_\alpha - \delta_{e_\alpha})).\end{aligned} \tag{24}$$

Since $\epsilon > 0$ and $\delta_e \to 0$, $\bar{m}(t)$ has a limited value. To achieve $dV/dt < 0$ in (24), the two adjustable gains k and $\bar{m}(t)$ should satisfy

$$\begin{cases} k > \max\left(\left|\frac{R_s}{L_s}D - gu_{n\alpha}\right|, \left|\frac{R_s}{L_s}D - gu_{n\beta}\right|\right) \\ \bar{m}(t) > \max\left(\frac{|\hat{\omega}_e(t)\delta_{e_\beta}(t)| + \delta_{\omega_e}(\hat{e}_\beta + \delta_{e_\beta})}{\epsilon + |s_\alpha(t)|^a}, \right. \\ \qquad\qquad \left. \frac{|\hat{\omega}_e(t)\delta_{e_\alpha}(t)| + \delta_{\omega_e}(\hat{e}_\beta + \delta_{e_\beta})}{\epsilon + |s_\beta(t)|^a}\right). \end{cases} \tag{25}$$

Considering the bounded nature of the term $|\delta_{\omega_e}(\hat{e} + \delta_e)|/(\epsilon + |s|^a)$, we redefine the adaptive gain as follows:

$$\bar{m}(t) = \bar{m}(t_0) + \max\left(\frac{|\hat{\omega}_e(t)\delta_{e_\beta}(t)|}{\epsilon + |s_\alpha(t)|^a}, \frac{|\hat{\omega}_e(t)\delta_{e_\alpha}(t)|}{\epsilon + |s_\beta(t)|^a}\right) \tag{26}$$

where $\bar{m}(t_0)$ represents the initial value of the adaptive gain at time t_0.

To ensure sufficient stability margin, the condition $\bar{m}(t_0) > E$ must be satisfied, where E is a positive constant that guarantees adequate damping against system uncertainties and perturbations.

In real applications, the stator resistance R_s and stator inductance L_s of a PMSM may drift due to temperature rise and magnetic saturation. Therefore, merely satisfying (25) may lead to system instability. In fact, the mismatch range of stator resistance R_s and stator inductance L_s in real applications is within 0.2 p.u. From (25), it can be seen that stator resistance R_s and stator inductance L_s mainly affect the range of k. Hence, considering the extreme case where the mismatch range of stator resistance R_s and stator inductance L_s is 0.2 p.u., k must satisfy the following condition:

$$k > \max\left(\frac{3R_s}{2L_s}D + |gu_{n\alpha}|, \frac{3R_s}{2L_s}D + |gu_{n\beta}|\right). \tag{27}$$

Based on the stability analysis, selecting appropriate k, $\bar{m}(t)$, and a can ensure the observe stability. Moreover, by introducing s, the equivalent gain coefficient can adaptively change in real-time, effectively reducing chattering and improving back-EMF estimation accuracy.

C. Chattering Attenuation Analysis of GA-HOTSMO

To evaluate the chattering suppression effectiveness of the proposed GA-HOTSMO, a comprehensive analysis of the estimated back-EMF $\hat{e}$ and the high-order terminal sliding mode control inputs $Z_{\boldsymbol{i}}$ and $\bar{\Delta}$ is conducted, comparing them with those of the traditional HOTSMO.

From (13), the estimated back-EMF $\hat{\mathbf{e}}$ based on GA-HOTSMO can be expressed as follows:

$$\hat{\mathbf{e}} = \int \left(\hat{\boldsymbol{A}}_{\mathbf{22}} \hat{\boldsymbol{e}} + M(\boldsymbol{s}, t)\text{sign}(\boldsymbol{s}) \right) dt. \tag{28}$$

In (28), the integration operation on discontinuous control law $\bar{\Delta}$ provides a smoothing effect on the back-EMF estimation, thereby mitigating the chattering phenomenon.

The high-order terminal sliding mode control rate $Z_{\mathbf{i}}$ of the designed GA-HOTSMO is same to that of HOTSMO, as shown in (6). The term $\mathbf{u}_n$ can be expressed as follows:

$$\mathbf{u}_n = \frac{k}{s+g}\text{sign}(\mathbf{s}) \tag{29}$$

where $\frac{k}{s+g}$ represents a standard LPF model with g as the equivalent cutoff frequency, enabling smooth control signals despite the inherent discontinuities of sliding mode control.

The distinctive feature of GA-HOTSMO lies in its adaptive gain coefficient $M(\boldsymbol{s}, t)$, which evolves dynamically based on the sliding mode surface $\boldsymbol{s}$ and adaptive function $\bar{m}(t)$ according to (14). The adaptive mechanism exhibits two characteristic phases as follows.

1) Dynamic response in reaching phase: For large magnitude of $\boldsymbol{s}$, $M(\boldsymbol{s}, t)$ maintains sufficient amplitude to satisfy the reaching condition, thereby ensuring robust convergence and observer stability.

2) Performance in sliding phase: As $\boldsymbol{s}$ converges to the sliding surface, $M(\boldsymbol{s}, t)$ adaptively decreases to an appropriate value, effectively suppressing the chattering phenomenon while preserving estimation accuracy.

In the presence of disturbances (e.g., load changes), $\boldsymbol{s}$ and $\bar{m}(t)$ increase synchronously, elevating $M(\boldsymbol{s}, t)$ to meet stability conditions (25). Subsequently, as observation errors converge, $\boldsymbol{s}$ decreases naturally, prompting $\bar{m}(t)$ to reduce $M(\boldsymbol{s}, t)$, thereby achieving chattering suppression while maintaining system stability.

As demonstrated in Fig. 3, the proposed GA-HOTSMO significantly reduces the chattering range of $\delta_{\mathbf{e}}$ compared to traditional HOTSMO, thereby enhancing back-EMF estimation accuracy.

D. Finite-Time Convergence Analysis of GA-HOTSMO

One of the main objectives in designing the GA-HOTSMO observer is to achieve finite-time convergence. According to Lyapunov stability theory, by selecting appropriate values for k and $\bar{m}(t)$ as indicated in (26) and (27), the system dynamics can converge to the sliding mode surface $\mathbf{s}$ in finite time and remain on this surface thereafter. Under this condition, equation (11) can be expressed as follows:

$$\frac{d}{dt}\begin{bmatrix}\delta_{i_\alpha}\\ \delta_{i_\beta}\end{bmatrix} = -\beta \begin{bmatrix}|\delta_{i_\alpha}|^{\gamma}\text{sign}(\delta_{i_\alpha})\\ |\delta_{i_\beta}|^{\gamma}\text{sign}(\delta_{i_\beta})\end{bmatrix}. \tag{30}$$

According to the finite-time stability theory of the error system [32], given initial conditions where $\delta_{\mathbf{i}}(0) \neq 0$, it is possible to ensure that $\delta_{\mathbf{i}}$ converges to zero in finite time by appropriately choosing the values of β and γ [24]. When the sliding mode surface $\mathbf{s} = 0$, $\delta_{\mathbf{i}} = 0$, implying that the derivative of the current error $\frac{d\delta_{\mathbf{i}}}{dt} = 0$.

From [33], the convergence time of the stator current error is given by

$$t = \frac{1}{\beta(1-\gamma)}\delta_{\boldsymbol{i}}(0)^{1-\gamma} \tag{31}$$

where $\delta_{\boldsymbol{i}}(0)$ represents the stator current error at the moment when the system state is disturbed (e.g., during load changes on the motor).

The GA-HOTSMO observer also ensures the convergence of the estimated back-EMF term. As discussed in [26], the error in the back-EMF term can be expressed as

$$\delta_{\boldsymbol{e}} = A_{12}^{-1}\left(\frac{d\delta_{\boldsymbol{i}}}{dt} - A_{11}\delta_{\boldsymbol{i}} + \beta\left|\delta_{\boldsymbol{i}}\right|^{\gamma}\text{sgn}(\delta_{\boldsymbol{i}}) + \boldsymbol{u}_n \right). \tag{32}$$

When $s = 0$, it follows from (6) and (30) that $\boldsymbol{u}_n = 0$ and $\delta_{\boldsymbol{i}} = 0$. Substituting these into (32) yields $\delta_{\boldsymbol{e}} = 0$.

In conclusion, the GA-HOTSMO observer guarantees finite-time convergence of the entire system, including both the current error and its derivative as well as the back-EMF error, significantly enhancing the accuracy of motor speed estimation.

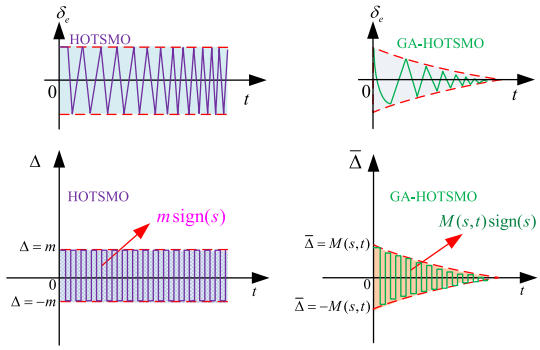

Fig. 3. Comparison of control inputs and chattering curves under HOTSMO and GA-HOTSMO.

IV. Implementation of the Proposed GA-HOTSMO

In this section, a systematic approach for tuning the GA-HOTSMO parameters is presented. Subsequently, a method for obtaining the derivative of the current error signal is proposed, employing the Savitzky–Golay filter.

A. Parameter Tuning of GA-HOTSMO

The performance of the proposed GA-HOTSMO observer depends critically on the appropriate selection of its parameters: β, γ, g, k, ϵ, a, and $\bar{m}(t)$. These parameters must be tuned to balance convergence speed, chattering suppression, and overall system stability. The tuning guidelines are as follows.

1) Parameter β: Influences the convergence rate and stability of the sliding mode surface. A larger β accelerates convergence but may increase chattering. It should be selected to balance rapid convergence with chattering mitigation.

2) Parameter γ: Determines the nonlinearity of the sliding mode surface. Lower values of γ enhance convergence speed but can exacerbate chattering, while higher values smooth the control signal but slow down convergence. A common choice is $\gamma = 0.5$, offering a compromise between responsiveness and stability [28].

3) Parameter g: Acts as an LPF coefficient in the control law, affecting dynamic response and noise attenuation. Smaller values improve noise suppression but reduce responsiveness; larger values enhance responsiveness but may increase chattering. g should balance noise filtering with dynamic performance.

4) Parameter k: Affects the amplitude of the control input. Increasing k enhances disturbance rejection and dynamic response but may lead to overshoot and oscillations. k should satisfy the stability condition in (27) and be tuned to achieve a balance between performance and stability.

5) Parameter ϵ: A small positive constant used to prevent division by zero in the adaptive gain function. Typically set to a negligible value (e.g., $\epsilon = 0.001$) with minimal impact on system dynamics.

6) Parameter a and $\bar{m}(t)$: Play significant roles in chattering suppression and convergence speed. The exponent a influences how the sliding surface function $\mathbf{s}$ affects the adaptive gain $M(\mathbf{s}, t)$, with a typical range between 0.5 and 1.5. The adaptive gain $\bar{m}(t)$ adjusts $M(\mathbf{s}, t)$ in real-time, enhancing responsiveness when necessary. However, excessive $\bar{m}(t)$ may increase chattering. Therefore, a and $\bar{m}(t)$ should be tuned jointly to balance convergence speed and chattering suppression.

In practical implementation, it is not feasible to manually adjust all parameters during operation. Parameters such as β, γ, g, k, and ϵ can be fixed based on design considerations and simulation results. The adaptive gain $\bar{m}(t)$ adjusts automatically during operation and does not require manual tuning. Parameter a may require fine-tuning during experimental validation to account for model uncertainties and achieve the desired performance.

B. Robust Current Error Derivative Estimation of GA-HOTSMO

To enhance the performance of the proposed GA-HOTSMO approach, a robust method for estimating the derivative of the current error, $\delta_{\mathbf{i}}$, is implemented. This method combines Savitzky–Golay filtering with an adaptive noise thresholding mechanism to mitigate noise effects and ensure stable derivative estimates, as illustrated in Fig. 4.

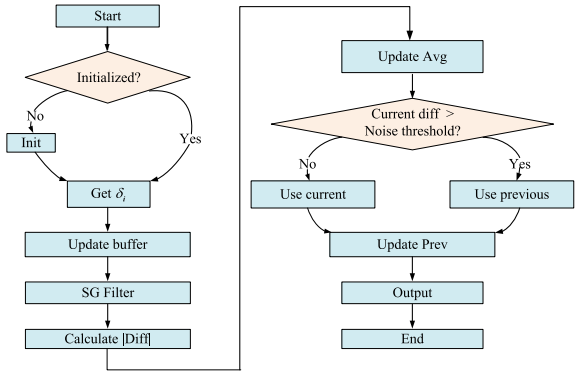

Fig. 4. Flowchart of Savitzky–Golay filtering and adaptive noise threshold for current error derivative.

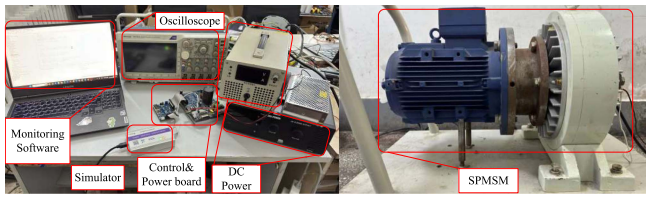

Fig. 5. Experimental platform.

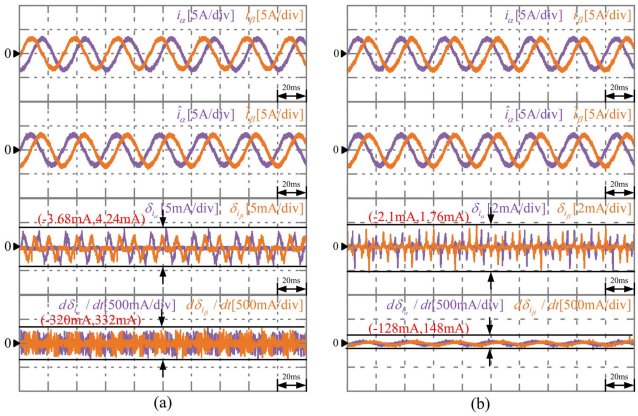

Fig. 6. Actual current, estimated current, current error, and derivative of current error at 3 N.m load torque and 500 r/min motor speed. (a) HOTSMO. (b) GA-HOTSMO.

The Savitzky–Golay filter utilizes a five-point window to approximate the first derivative of the current estimation error. Precomputed filter coefficients of $[-2, -1, 0, 1, 2]/10$ are applied to a rolling buffer of the five most recent values of $\delta_{\mathbf{i}}$. The computed derivative is expressed as follows:

$$\frac{d\delta_{\mathbf{i}}}{dt} = \sum_{i=1}^{5} c_i \cdot \delta_{\mathbf{i},i} \tag{33}$$

where c_i represents the ith coefficient, and $\delta_{\mathbf{i},i}$ is the ith most recent error value in the buffer. This approach effectively smoothens the current error signal, minimizing

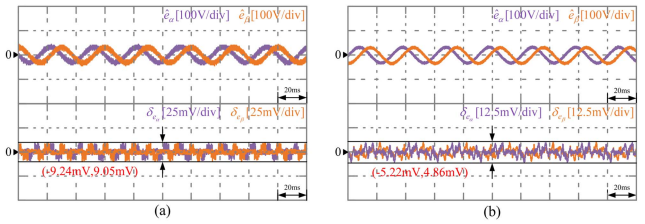

Fig. 7. Estimated back-EMF and back-EMF error at 3 N.m load torque and 500 r/min motor speed. (a) HOTSMO. (b) GA-HOTSMO.

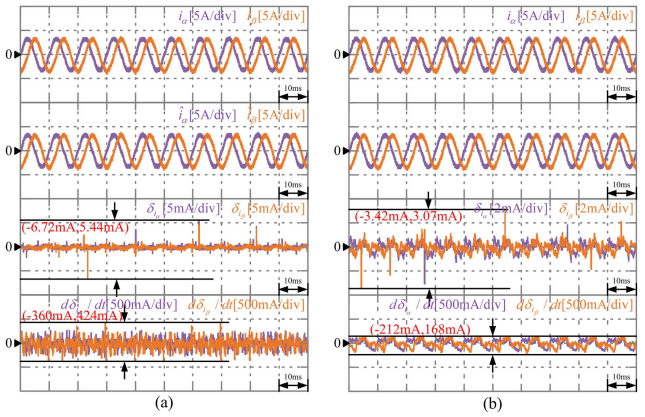

Fig. 8. Actual current, estimated current, current error, and derivative of current error at 3 N.m load torque and 1500 r/min motor speed. (a) HOTSMO. (b) GA-HOTSMO.

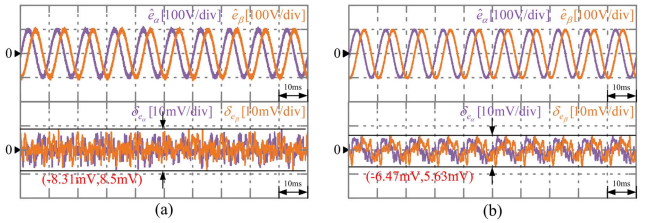

Fig. 9. Estimated back-EMF and back-EMF error at 3 N.m load torque and 1500 r/min motor speed. (a) HOTSMO. (b) GA-HOTSMO.

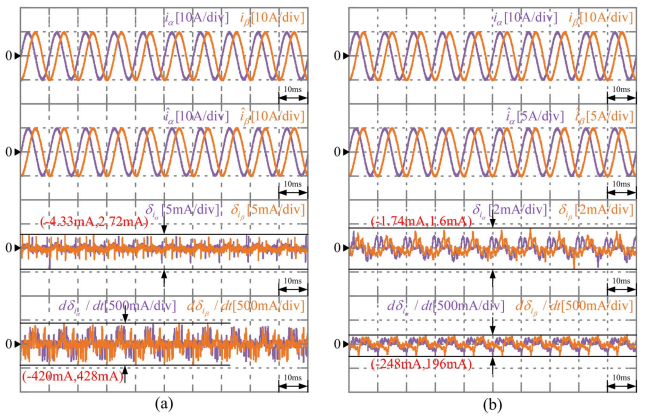

Fig. 10. Actual current, estimated current, current error, and derivative of current error at 9 N.m load torque and 1500 r/min motor speed. (a) HOTSMO. (b) GA-HOTSMO.

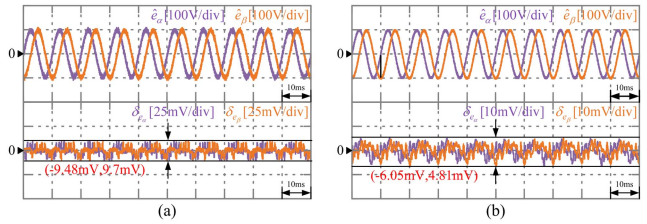

Fig. 11. Estimated back-EMF and back-EMF error at 9 N.m load torque and 1500 r/min motor speed. (a) HOTSMO. (b) GA-HOTSMO.

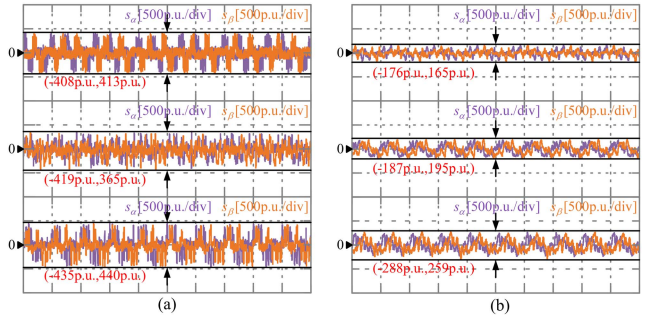

Fig. 12. Sliding mode surface function $\mathbf{s}$ curves under three different operating conditions. From top to bottom: load torque of 3 N.m at a motor speed of 500 r/min, load torque of 3 N.m at a motor speed of 1500 r/min, and load torque of 9 N.m at a motor speed of 1500 r/min. (a) HOTSMO. (b) GA-HOTSMO.

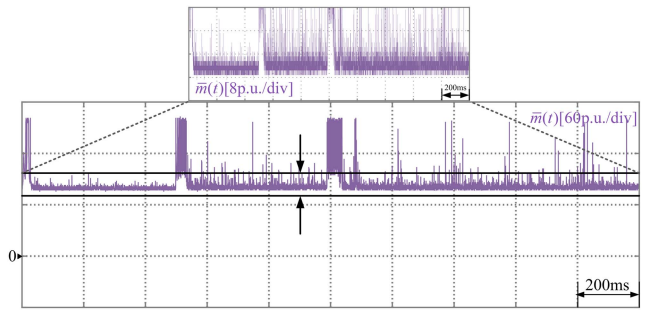

Fig. 13. Adaptive gain $\bar{m}(t)$ during load and speed changes from 3 N.m at 500 r/min to 3 N.m at 1500 r/min, followed by load variations between 3 and 9 N.m at 1500 r/min.

the amplification of high-frequency noise during derivative calculation.

To further mitigate the impact of sudden noise spikes, an adaptive noise thresholding mechanism is employed alongside the Savitzky–Golay filter. An exponentially weighted moving average (EMA) of the absolute derivative values is maintained to estimate the average rate of change of the current error

$$\mathrm{EMA}_t = (1-\alpha)\cdot \mathrm{EMA}_{t-1} + \alpha \cdot \left| \frac{d\delta_{\mathbf{i}}}{dt} \right|_t \tag{34}$$

where α is the smoothing factor. If the current derivative exceeds a threshold defined by the EMA and a sensitivity factor λ, the

TABLE I
SPMSM PARAMETERS

Parameters	Value
Rated power/kw	2.3
Rated voltage/V	220
Rated current/A	9.5
Stator resistance/Ω	1.1
D-axis and Q-axis	4.45
Permanent magnet flux/Wb	0.158
Rated torque/N·m	9
Pole pairs/P	4
Switching frequency/kHz	10

previous output value is retained

$$\text{output} = \begin{cases} \frac{d\delta_i}{dt}, & \text{if } \left|\frac{d\delta_i}{dt}\right| \le \lambda \cdot \text{EMA}_t \\ \text{previous output}, & \text{otherwise.} \end{cases} \tag{35}$$

This combined approach provides effective noise suppression and stable derivative estimation, ensuring reliable performance in real-time control applications.

V. Experimental Verification

To validate the proposed GA-HOTSMO, a 2.3 kW SPMSM experimental platform was constructed, as shown in Fig. 5. The torque of the SPMSM is controlled by a magnetic powder brake. The control algorithm is executed on a 32-bit fixed-point microcontroller, the TMS320F28027, from Texas Instruments. The power converter consists of a dc power supply and an inverter.

The control methods are the SVC of the PMSM with the GA-HOTSMO and the HOTSMO, respectively. The parameters of GA-HOTSMO are set as $k = 120$, $g = 600$, $\beta = 100$, $\gamma = 0.5$, $a = 0.86$, $\epsilon = 0.001$, the adaptive adjustment coefficient $\bar{m}(t_0) = 80$. The parameters of HOTSMO are set as $k = 120$, $g = 600$, $\beta = 100$, $\gamma = 0.5$, the fixed gain coefficient $m = 2000$ which is the minimum value that ensures the stability of the observer. For the SPMSM drive based on FOC, the current loop bandwidth is set to 600 Hz, the operating frequency of the orthogonal PLL is set to 200 Hz [27], and the cutoff frequency and phase margin of the speed loop are set to 38 Hz and 81°, respectively. Table I shows the parameters of the SPMSM used in the experiment.

A. Steady-State Performance Verification

Figs. 6 and 7 show the experimental results observed by two observers when the load torque is 3 N.m and the SPMSM runs at 500 r/min. Figs. 8 and 9 show the experimental results observed by two observers when the load torque is 3 N.m and the SPMSM runs at 1500 r/min. Figs. 10 and 11 show the experimental results observed by two observers when the load torque is 9 N.m and the SPMSM runs at 1500 r/min. The curves are, in order, actual current, estimated current, current error, derivative of current error, motor back-EMF, and back-EMF error.

As shown in Figs. 6, 8, and 10, the actual and estimated currents observed by both HOTSMO and GA-HOTSMO are generally consistent, but the current observed by GA-HOTSMO is more accurate. This is evidenced by the current error and its derivative. When the load torque is 3 N.m and the SPMSM runs at 500 r/min, the current error range estimated by HOTSMO is $\delta_i \in (-3.68\text{ mA}, 4.24\text{ mA})$, and the derivative of the estimated current error ranges from $(-320\text{ mA}, 332\text{ mA})$. In contrast, the current error range observed by GA-HOTSMO is $\delta_i \in (-2.10\text{ mA}, 1.76\text{ mA})$, with the derivative of the estimated current error ranging from $(-128\text{ mA}, 148\text{ mA})$. When the load torque is 3 N.m and the SPMSM runs at 1500 r/min, the current error range estimated by HOTSMO is $\delta_i \in (-6.72\text{ mA}, 5.44\text{ mA})$, with the derivative of the estimated current error ranging from $(-360\text{ mA}, 424\text{ mA})$. Meanwhile, the current error range observed by GA-HOTSMO is $\delta_i \in (-3.42\text{ mA}, 3.07\text{ mA})$, with the derivative of the estimated current error ranging from $(-212\text{ mA}, 168\text{ mA})$. When the load torque is 9 N.m and the SPMSM runs at 1500 r/min, the current error range estimated by HOTSMO is $\delta_i \in (-4.33\text{ mA}, 2.72\text{ mA})$, with the derivative of the estimated current error ranging from $(-420\text{ mA}, 428\text{ mA})$. In contrast, the current error range observed by GA-HOTSMO is $\delta_i \in (-1.74\text{ mA}, 1.6\text{ mA})$, with the derivative of the estimated current error ranging from $(-248\text{ mA}, 196\text{ mA})$. These results indicate that the current error observed by GA-HOTSMO is smaller, allowing it to quickly and accurately observe the stator current and ensure the accuracy of the back-EMF estimation. Furthermore, the difference in the derivatives of the estimated current errors between GA-HOTSMO and HOTSMO is particularly significant, greatly enhancing the accuracy of the motor speed estimation.

As shown in Figs. 7, 9, and 11, the estimated back-EMF values obtained by HOTSMO and GA-HOTSMO are generally consistent, but the back-EMF values observed by GA-HOTSMO are more accurate, as evidenced by the comparison of back-EMF errors. When the load torque is 3 N.m and the SPMSM runs at 500 r/min, the range of back-EMF error estimated by HOTSMO is $\delta_e \in (-9.24\text{ mV}, 9.05\text{ mV})$, while the back-EMF error range observed by GA-HOTSMO is $\delta_e \in (-5.22\text{ mV}, 4.86\text{ mV})$. When the load torque is 3 N.m and the SPMSM runs at 1500 r/min, the range of back-EMF error estimated by HOTSMO is $\delta_e \in (-8.31\text{ mV}, 8.5\text{ mV})$, while the back-EMF error range observed by GA-HOTSMO is $\delta_e \in (-6.47\text{ mV}, 5.63\text{ mV})$. When the load torque is 9 N.m and the SPMSM runs at 1500 r/min, the range of back-EMF error estimated by HOTSMO is $\delta_e \in (-9.48\text{ mV}, 9.7\text{ mV})$, while the back-EMF error range observed by GA-HOTSMO is $\delta_e \in (-6.05\text{ mV}, 4.81\text{ mV})$. The experimental results show that the back-EMF error observed by GA-HOTSMO is significantly smaller than that observed by HOTSMO. Since GA-HOTSMO can more accurately observe the current and back-EMF, the PLL can more accurately extract the speed and rotor position information from the back-EMF.

Fig. 12 shows the sliding mode surface function $\mathbf{s}$ waveforms for both HOTSMO and GA-HOTSMO. The curves from top to bottom represent the sliding mode surface function waveforms under the following conditions: a load torque of 3 N.m

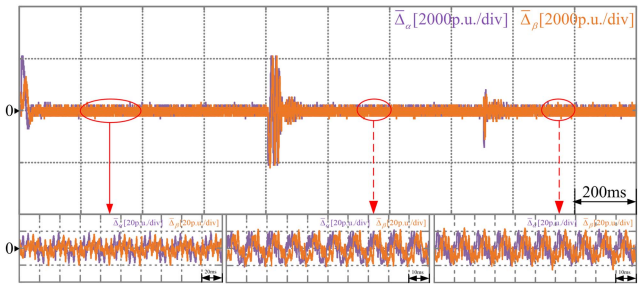

Fig. 14. Control input $\bar{\Delta}$ variation curves when the load torque changes from 3 N.m at 500 r/min to 3 N.m at 1500 r/min, and then to 9 N.m at 1500 r/min.

at a motor speed of 500 r/min, a load torque of 3 N.m at a motor speed of 1500 r/min, and a load torque of 9 N.m at a motor speed of 1500 r/min. When the load torque is 3 N.m and the SPMSM runs at 500 r/min, the range of the sliding mode surface function $\mathbf{s}$ observed by HOTSMO is $\mathbf{s} \in (-408\ \text{p.u.}, 413\ \text{p.u.})(1\ \text{p.u.} = 0.001)$, while the range observed by GA-HOTSMO is $\mathbf{s} \in (-176\ \text{p.u.}, 165\ \text{p.u.})$. When the load torque is 3 N.m and the SPMSM runs at 1500 r/min, the range of the sliding mode surface function $\mathbf{s}$ observed by HOTSMO is $\mathbf{s} \in (-419\ \text{p.u.}, 365\ \text{p.u.})$, while the range observed by GA-HOTSMO is $\mathbf{s} \in (-187\ \text{p.u.}, 195\ \text{p.u.})$. When the load torque is 9 N.m and the SPMSM runs at 1500 r/min, the range of the sliding mode surface function $\mathbf{s}$ observed by HOTSMO is $\mathbf{s} \in (-435\ \text{p.u.}, 440\ \text{p.u.})$, while the range observed by GA-HOTSMO is $\mathbf{s} \in (-288\ \text{p.u.}, 259\ \text{p.u.})$. The results indicate that, in steady state, the GA-HOTSMO exhibits a smaller range of chattering in the sliding mode surface function $\mathbf{s}$ compared to the HOTSMO under various load conditions and motor speeds. This means that the GA-HOTSMO can more effectively suppress chattering while maintaining stability.

B. Transient Performance Verification

Figs. 13 and 14 illustrate the variation in the adaptive gain $\bar{m}(t)$ and the control input $\bar{\Delta}$ during load and speed changes, where 1 p.u. $= 1$. Specifically, Fig. 13 presents the adaptive gain $\bar{m}(t)$ variations under speed transitions from 500 to 1500 r/min at constant torque (3 N.m), followed by load torque variations between 3 and 9 N.m at 1500 r/min. The adaptive gain is initialized at $\bar{m}(t_0) = 80$ and exhibits dynamic responses to system state changes. During transient processes caused by speed and load variations, $\bar{m}(t)$ increases rapidly to compensate for estimation errors, thereby ensuring fast convergence and enhanced disturbance rejection capability. The corresponding control input $\bar{\Delta}$ generated by the GA-HOTSMO with variable gain coefficient $M(\mathbf{s}, t)$ is illustrated in Fig. 14. The gain coefficient adapts to system states in real-time: increasing when state variables deviate significantly from the sliding surface to maintain stability, and decreasing as states approach the sliding surface to minimize chattering. This adaptive mechanism effectively balances control performance and chattering suppression.

The coordinated behavior between $\bar{m}(t)$ and $\bar{\Delta}$ validates the proposed adaptive strategy. The rapid adaptation of $\bar{m}(t)$ during

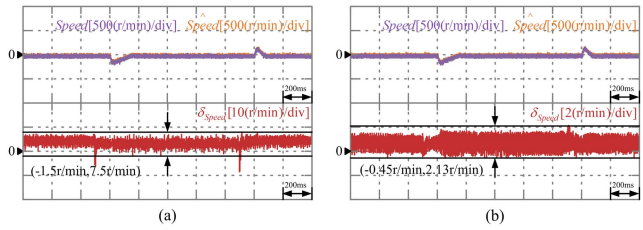

Fig. 15. Motor speed and speed error when load torque changes at 1000 r/min. (a) HOTSMO. (b) GA-HOTSMO.

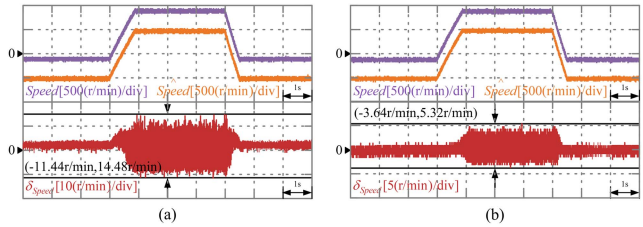

Fig. 16. Motor speed and speed error when accelerating and decelerating. (a) HOTSMO. (b) GA-HOTSMO.

transients directly enhances the disturbance rejection capability of $\bar{\Delta}$. Although adaptive smoothing is applied to the current error derivative $d\delta_{\mathbf{i}}/dt$ in sliding mode, $\bar{m}(t)$ still exhibits certain high-frequency fluctuations. However, as evidenced in Fig. 14, these fluctuations have minimal impact on $\bar{\Delta}$, which maintains stable operation without inducing excessive chattering, thereby ensuring robust system performance.

Fig. 15 shows the experimental results of the SPMSM at a speed of 1000 r/min under different load torques, including the actual motor speed, estimated speed, and speed error. The load torque jumps from 3 to 9 N.m during loading and from 9 N.m back to 3 N.m during unloading. Under different load torque conditions, the speed error range observed using HOTSMO is $\delta_{\text{Speed}} \in (-1.5\ \text{r/min}, 7.5\ \text{r/min})$. In contrast, the speed error range observed using GA-HOTSMO is $\delta_{\text{Speed}} \in (-0.45\ \text{r/min}, 2.13\ \text{r/min})$. The experimental data indicate that the speed error observed using GA-HOTSMO is significantly smaller than that observed using HOTSMO under different load torque conditions.

Fig. 16 presents the results of the motor speed changes observed under HOTSMO and GA-HOTSMO, including the actual motor speed, estimated speed, and speed error. During acceleration, the speed increases from 500 to 1500 r/min, and during deceleration, the speed decreases from 1500 to 500 r/min, with a load torque of 9 N.m. The speed error range obtained using HOTSMO is $\delta_{\text{Speed}} \in (-11.44\ \text{r/min}, 14.48\ \text{r/min})$. The speed error range obtained using GA-HOTSMO is $\delta_{\text{Speed}} \in (-3.64\ \text{r/min}, 5.32\ \text{r/min})$. The estimated speed and speed error clearly show that the speed oscillation error observed using GA-HOTSMO is significantly smaller than that observed using HOTSMO.

Moreover, Figs. 15 and 16 clearly demonstrate that the transient performance of the motor under both HOTSMO and GA-HOTSMO observers is almost identical, with both achieving

TABLE II
COMPARISON OF OBSERVER PERFORMANCE

	SMO [15]	ESMO [21]	HOTSMO [26]	GA-HOTSMO (proposed)
Chattering	Severe	Moderate	Mild	Negligible
Dynamic performance	Poor	Better	Good	Best
Convergence	No	No	Yes	Yes
Estimation accuracy	Low	Medium	High	Higher

TABLE III
COMPUTATIONAL BURDENS OF TWO DIFFERENT ALGORITHMS

Method	Computational operations		Computation time
	Algorithm	Operation count	
Conventional HOTSMO [26]	+,-	26	10.15 μs
	*,/	32	
	sqrt	2	
Proposed GA-HOTSMO	+,-	34	13.72 μs
	*,/	40	
	sqrt	4	

finite-time convergence. However, in terms of rotor position estimation accuracy, GA-HOTSMO shows superior performance.

C. Performance Comparison

The experiment aims to compare the performance between the HOTSMO observer and the GA-HOTSMO observer. Since the performance of HOTSMO far surpasses that of traditional SMO observers and ESMO, further discussion on these is omitted here [26]. Table II compares performance indicators of the traditional first-order SMO, extended SMO, HOTSMO, and GA-HOTSMO.

D. Computational Burden Evaluation

Table III compares the computational burden of the traditional HOTSMO and the proposed GA-HOTSMO. It is observed that the computation time of GA-HOTSMO is 13.72 μs, approximately 1.35 times that of HOTSMO. This increase in computation time is consistent with the added complexity of the adaptive gain mechanism in GA-HOTSMO. In this study, the control period is set to 100 μs; therefore, the computation time of GA-HOTSMO occupies about 13.72% of the control period. This computational load is well within the acceptable range for industrial applications, satisfying standard real-time processing requirements.

VI. CONCLUSION

In this article, the GA-HOTSMO is proposed to address the issues of chattering, nonfinite time convergence, and low estimation accuracy in traditional SMOs, extended SMOs, and traditional higher order SMOs for PMSM control systems. GA-HOTSMO effectively suppresses system chattering while ensuring the stability of the observer, which can more accurately observe the stator current and back-EMF information and thus improve the estimation accuracy of motor speed and rotor position. Experimental verification showed that the current error and back-EMF error observed by GA-HOTSMO were significantly reduced compared to HOTSMO, greatly improving the estimation accuracy of current and back-EMF while reducing system chattering. Therefore, by using the back-EMF observed by GA-HOTSMO, the rotor speed and position information can be more accurately extracted, thereby improving the control accuracy. GA-HOTSMO was verified in experiment to improve system performance in terms of chattering suppression, finite time convergence, estimation accuracy improvement, and dynamic performance improvement.

REFERENCES

[1] Y. Zuo, C. Lai, and K. L. V. Iyer, "A review of sliding mode observer based sensorless control methods for PMSM drive," *IEEE Trans. Power Electron.*, vol. 38, no. 9, pp. 11352–11367, Sep. 2023.
[2] A. K. Junejo, W. Xu, C. Mu, M. M. Ismail, and Y. Liu, "Adaptive speed control of PMSM drive system based a new sliding-mode reaching law," *IEEE Trans. Power Electron.*, vol. 35, no. 11, pp. 12110–12121, Nov. 2020.
[3] J. M. Liu and Z. Q. Zhu, "Sensorless control strategy by square-waveform high-frequency pulsating signal injection into stationary reference frame," *IEEE J. Emerg. Sel. Topics Power Electron.*, vol. 2, no. 2, pp. 171–180, Jun. 2014.
[4] G. Wang, M. Valla, and J. Solsona, "Position sensorless permanent magnet synchronous machine drives-a review," *IEEE Trans. Ind. Electron.*, vol. 67, no. 7, pp. 5830–5842, Jul. 2020.
[5] M. Boussak, "Implementation and experimental investigation of sensorless speed control with initial rotor position estimation for interior permanent magnet synchronous motor drive," *IEEE Trans. Power Electron.*, vol. 20, no. 6, pp. 1413–1422, Nov. 2005.
[6] D. Xiao, S. Nalakath, Y. Sun, J. Wiseman, and A. Emadi, "Complex-coefficient adaptive disturbance observer for position estimation of IPMSMs with robustness to DC errors," *IEEE Trans. Ind. Electron.*, vol. 67, no. 7, pp. 5924–5935, Jul. 2020.
[7] H. Kim, J. Son, and J. Lee, "A high-speed sliding-mode observer for the sensorless speed control of a PMSM," *IEEE Trans. Ind. Electron.*, vol. 58, no. 9, pp. 4069–4077, Sep. 2011.
[8] C. Gong, Y. Hu, J. Gao, Y. Wang, and L. Yan, "An improved delay-suppressed sliding-mode observer for sensorless vector-controlled PMSM," *IEEE Trans. Ind. Electron.*, vol. 67, no. 7, pp. 5913–5923, Jul. 2020.
[9] B. Wang, Z. Dong, Y. Yu, G. Wang, and D. Xu, "Static-errorless deadbeat predictive current control using second-order sliding-mode disturbance observer for induction machine drives," *IEEE Trans. Power Electron.*, vol. 33, no. 3, pp. 2395–2403, Mar. 2018.
[10] S. -C. Yang and Y. -L. Hsu, "Full speed region sensorless drive of permanentmagnet machine combining saliency-based and back-EMF-based drive," *IEEE Trans. Ind. Electron.*, vol. 64, no. 2, pp. 1092–1101, Feb. 2017.
[11] S. Po-ngam and S. Sangwongwanich, "Stability and dynamic performance improvement of adaptive full-order observers for sensorless PMSM drive," *IEEE Trans. Power Electron.*, vol. 27, no. 2, pp. 588–600, Feb. 2012.
[12] S. Jin, B. Wang, Y. Zhang, S. Liu, and W. Jin, "Improved sliding-mode observer for sensorless control of high speed permanent magnet synchronous motor," in *Proc. 23 rd Int. Conf. Elect. Machines Syst.*, Hamamatsu, Japan, 2020, pp. 1918–1923.
[13] N. K. Quang, N. T. Hieu, and Q. P. Ha, "FPGA-Based sensorless PMSM speed control using reduced-order extended Kalman filters," *IEEE Trans. Ind. Electron.*, vol. 61, no. 12, pp. 6574–6582, Dec. 2014.
[14] M. Morawiec and A. Lewicki, "Speed observer structure of induction machine based on sliding super-twisting and backstepping techniques," *IEEE Trans. Ind. Informat.*, vol. 17, no. 2, pp. 1122–1131, Feb. 2021.
[15] H. Lee and J. Lee, "Design of iterative sliding mode observer for sensorless PMSM control," *IEEE Trans. Control Syst. Technol.*, vol. 21, no. 4, pp. 1394–1399, Jul. 2013.
[16] Z. Wang, J. Wang, J. Zhao, and Z. Liu, "Switching gain adaptive sliding mode model-following speed control of PMSM," in *Proc. 29th Chin. Control Conf.*, Beijing, China, 2010, pp. 3238–3243.
[17] Q. Xu, "Adaptive integral terminal third-order finite-time sliding-mode strategy for robust nanopositioning control," *IEEE Trans. Ind. Electron.*, vol. 68, no. 7, pp. 6161–6170, Jul. 2021.
[18] D. Fu and X. Zhao, "A novel robust adaptive nonsingular fast integral terminal sliding mode controller for permanent magnet linear synchronous motors," *IEEE J. Emerg. Sel. Topics Power Electron.*, vol. 11, no. 2, pp. 1672–1683, Apr. 2023.

[19] C. J. V. Filho and R. P. Vieira, "Adaptive full-order observer analysis and design for sensorless interior permanent magnet synchronous motors drives," *IEEE Trans. Ind. Electron.*, vol. 68, no. 8, pp. 6527–6536, Aug. 2021.
[20] M. Comanescu, "Design of a MRAS-based estimator for the speed and rotor time constant of the induction motor using sliding mode," in *Proc. 2016 Int. Symp. Power Electron., Elect. Drives, Automat. Motion*, Capri, Italy, 2016, pp. 740–745.
[21] G. Wang, Z. Li, G. Zhang, Y. Yu, and D. Xu, "Quadrature PLL-based highorder sliding-mode observer for IPMSM sensorless control with online MTPA control strategy," *IEEE Trans. Energy Convers.*, vol. 28, no. 1, pp. 214–224, Mar. 2013.
[22] A. Wang, X. Jia, and S. Dong, "A new exponential reaching law of sliding mode control to improve performance of permanent magnet synchronous motor," *IEEE Trans. Magn.*, vol. 49, no. 5, pp. 2409–2412, May 2013.
[23] J. Lee, P. H. Chang, and M. Jin, "Adaptive integral sliding mode control with time-delay estimation for robot manipulators," *IEEE Trans. Ind. Electron.*, vol. 64, no. 8, pp. 6796–6804, Aug. 2017.
[24] B. Wang, C. Luo, Y. Yu, G. Wang, and D. Xu, "Antidisturbance speed control for induction machine drives using high-order fast terminal slidingmode load torque observer," *IEEE Trans. Power Electron.*, vol. 33, no. 9, pp. 7927–7937, Sep. 2018.
[25] Y. Feng, J. Zheng, X. Yu, and N. V. Truong, "Hybrid terminal sliding-mode observer design method for a permanent-magnet synchronous motor control system," *IEEE Trans. Ind. Electron.*, vol. 56, no. 9, pp. 3424–3431, Sep. 2009.
[26] B. Wang, Y. Shao, Y. Yu, Q. Dong, Z. Yun, and D. Xu, "High-order terminal sliding-mode observer for chattering suppression and finite-time convergence in sensorless SPMSM drives," *IEEE Trans. Power Electron.*, vol. 36, no. 10, pp. 11910–11920, Oct. 2021.
[27] Y. Zhang and J. Zhang, "An improved Q-PLL to overcome the speed reversal problems in sensorless PMSM drive," in *Proc. IEEE 8th Int. Power Electron. Motion Control Conf.*, 2016, pp. 1884–1888.
[28] S. Yu, X. H. Yu, and B. Shirinzadehc, "Continuous finite-time control for robotic manipulators with terminal sliding mode," *Automatica*, vol. 41, no. 11, pp. 1957–1964, Nov. 2005.
[29] M. S. Zaky, M. K. Metwaly, H. Z. Azazi, and S. A. Deraz, "A newadaptive SMO for speed estimation of sensorless induction motor drives at zero and very low frequencies," *IEEE Trans. Ind. Electron.*, vol. 65, no. 9, pp. 6901–6911, Sep. 2018.
[30] Z. Q. Chen, M. Tomita, S. Doki, and S. Okuma, "An extended electromotive force model for sensorless control of interior permanent magnet synchronous motors," *IEEE Trans. Ind. Electron.*, vol. 50, no. 2, pp. 288–295, Apr. 2003.
[31] Z. Chen, M. Tomita, S. Doki, and S. Okuma, "New adaptive sliding observers for position- and velocity-sensorless controls of brushless dc motors," *IEEE Trans. Ind. Electron.*, vol. 47, no. 3, pp. 582–591, Jun. 2000.
[32] Y. Hong, J. Huang, and Y. Xu, "On an output feedback finite-time stabilization problem," *IEEE Trans. Automat. Control*, vol. 46, no. 2, pp. 305–309, Feb. 2001.
[33] S. P. Bhat and D. S. Bernstein, "Finite-time stability of homogeneous systems," in *Proc. Amer. Control Conf.*, 1997, pp. 2513–2514.

Chonghui Song (Member, IEEE) received the B.S. degree in fluid machine engineering from Xi'an Jiaotong University, Xi'an, China, in 1996, and the M.S. and Ph.D. degrees in automatic control theory and engineering from Northeastern University, Shenyang, China, in 1999 and 2004, respectively.

He is currently an Associate Professor with the College of Information Science and Engineering, Northeastern University. From 2006 to 2008, he was a Visiting Scholar with the Department of Electrical and Computer Engineering, University of Illinois at Chicago, Chicago, IL, USA. His research interests include power electronics, optimal control, differential game, and dynamic programming.

Wenbing Hu received the B.S. degree in electric engineering from the College of Information Science and Engineering, Northeastern University, Shenyang, China, in 2021, where he is currently working toward the Ph.D. degree in electric engineering.

His research interests include power electronics, ac motor drives, sensorless control, nonlinear control theory, and dc/dc converters.

Jiayan Zhang was born in Liaoning Province, China, in 2003. She is currently working toward the B.S. degree in control science and engineering with the College of Information Science and Engineering, Northeastern University, Shenyang, China.

Her research interests include ac motor drives, optimal control, and machine learning.

Chunwang Zhao was born in Henan Province, China, in 1996. He received the B.S. degree from the Shenyang University of Technology, Shenyang, China, in 2020, and the M.S. degree from Northeastern University, Shenyang, China, in 2023, both in electrical engineering.

He is currently engaged in related professional work in an enterprise. His research interests include motors drives and sensorless control.

Xianrui Sun received the M.S. degree in power electronics and electrical drives and the Ph.D. degree in electrical engineering from Northeastern University, Shenyang, China, in 2013 and 2023, respectively.

He is currently the Lecturer and Master Supervisor with the College of Information Engineering, Shenyang University of Chemical Technology, Shenyang, China. His research interests include power electronics, dc/ac converters, and multilevel converters.